Clim Dyn
DOI 10.1007/s00382-017-3893-5

Tropically driven and externally forced patterns of Antarctic sea ice change: reconciling observed and modeled trends

David P. Schneider[1] · Clara Deser[1]

Received: 7 February 2017 / Accepted: 28 August 2017

Abstract Recent work suggests that natural variability has played a significant role in the increase of Antarctic sea ice extent during 1979–2013. The ice extent has responded strongly to atmospheric circulation changes, including a deepened Amundsen Sea Low (ASL), which in part has been driven by tropical variability. Nonetheless, this increase has occurred in the context of externally forced climate change, and it has been difficult to reconcile observed and modeled Antarctic sea ice trends. To understand observed-model disparities, this work defines the internally driven and radiatively forced patterns of Antarctic sea ice change and exposes potential model biases using results from two sets of historical experiments of a coupled climate model compared with observations. One ensemble is constrained only by external factors such as greenhouse gases and stratospheric ozone, while the other explicitly accounts for the influence of tropical variability by specifying observed SST anomalies in the eastern tropical Pacific. The latter experiment reproduces the deepening of the ASL, which drives an increase in regional ice extent due to enhanced ice motion and sea surface cooling. However, the overall sea ice trend in every ensemble member of both experiments is characterized by ice loss and is dominated by the forced pattern, as given by the ensemble-mean of the first experiment. This pervasive ice loss is associated with a strong warming of the ocean mixed layer, suggesting that the ocean model does not locally store or export anomalous heat efficiently enough to maintain a surface environment conducive to sea ice expansion. The pervasive upper-ocean warming, not seen in observations, likely reflects ocean mean-state biases.

Keywords Antarctica · Southern Ocean · Sea ice · Models · Climate variability and change

Electronic supplementary material The online version of this article (doi:10.1007/s00382-017-3893-5) contains supplementary material, which is available to authorized users.

✉ David P. Schneider
dschneid@ucar.edu

[1] Climate and Global Dynamics Laboratory, National Center for Atmospheric Research, Boulder, CO, USA

1 Introduction

The modest increase in Antarctic sea ice extent (SIE), apparent since the late 1990s and continuing through at least 2015 (Parkinson and DiGirolamo 2016), has been an enigma in a warming world. The observed increase generally contradicts expectations from climate model experiments (e.g. Turner et al. 2013; Hobbs et al. 2015; Jones et al. 2016). Recent work towards resolving this paradox points to (a) the large interannual-to-interdecadal climate variability of Antarctica and the Southern Ocean (Turner et al. 2016; Jones et al. 2016; Fan et al. 2014; Polvani and Smith 2013) that may mask any forced changes; (b) the specific role of tropical teleconnections in this variability, notably a shift in the phase of the Pacific Decadal Oscillation (PDO, also referred to as the Interdecadal Pacific Oscillation or IPO) in 1998–1999, which has led to a deepened ASL (Meehl et al. 2016; Purich et al. 2016; Raphael et al. 2016); (c) the uncertain response of the Southern Ocean to the stronger westerly winds associated with polar stratospheric ozone depletion, which depends on the timescale and model examined (Ferreira et al. 2015; Kostov et al. 2016); and (d) the role played by processes not well observed nor routinely represented in models, such as freshening of the Southern Ocean from the melting of ice shelves and glacial ice (e.g. Bintanja et al. 2013; Swart and Fyfe 2013). Some authors have questioned the reality of the trend in the observational record of Antarctic sea ice extent (Eisenman et al. 2014), while others have found that additional indicators, including sea surface temperatures (SSTs) and near-surface winds, have changed in a way that is consistent with the hemispheric and regional SIE trends (Fan et al. 2014; Armour and Bitz 2015). The strong covariance of SIE with SST and near-surface winds on interannual-to-interdecadal timescales suggests that the increase in SIE is part of a large-scale, systematic pattern. As such, explanations for the increase in Antarctic SIE should also account for the trends in SSTs and winds (Fan et al. 2014; Armour and Bitz 2015). Many explanations for the trend in SIE were reviewed in Armour and Bitz (2015) and Hobbs et al. (2016), and both studies concluded that large-scale atmospheric circulation changes are the most likely cause of the observed Antarctic sea ice trends.

Recent trends in the large-scale atmospheric circulation over the Southern Ocean were interpreted by Schneider et al. (2015), who used a series of atmospheric modeling experiments to show that the spatial and seasonal aspects of zonal wind trends could be explained by a combination of stratospheric ozone depletion, tropical teleconnections, and intrinsic variability. Specifically, wind anomalies in the south Pacific during the non-summer months can be reproduced in atmospheric model experiments forced only with time-varying, observed tropical SST anomalies. Zonal-mean westerly wind trends in austral summer, reflected in the positive trend of the Southern Annular Mode (SAM), are best explained if stratospheric ozone depletion is included in the model simulation. In turn, these wind trends have impacted Southern Ocean SST trends. The sequence of Southern Ocean SST anomalies during 1979–2014 can be empirically modeled as a response to circulation trends associated with the El Niño-Southern Oscillation (ENSO) and the SAM (Yeo and Kim 2015).

Given the previous interpretations of the wind and SST trends, a logical extension of the conclusion of Armour and Bitz (2015) and Hobbs et al. (2016) is that atmospheric circulation trends, driven by a combination of tropical teleconnections and external forcing including stratospheric ozone, have caused the observed Antarctic sea ice trends. We note that this argument dates back in various forms to at least Liu et al. (2004). Part of the problem in accepting this hypothesis is that the sea ice trends that are congruent with common indices of the atmospheric circulation are weaker than the actual sea ice trends and do not fully explain the spatial pattern (e.g. Liu et al. 2004; Matear et al. 2015; Simpkins et al. 2013; Hobbs et al. 2016). This is perhaps due to the complexity of atmosphere-ocean-sea ice interactions that cannot be captured in simple regression statistics. In addition, SAM and ENSO-related anomalies do not account for all of the atmospheric circulation variability that may be important to sea ice trends (Matear et al. 2015). As empirical regression models may have limited value in such a complex system, coupled climate models may be better suited to understanding the response of sea ice to atmospheric forcing. However, to date, there have been relatively few studies with coupled models of the linkages between atmospheric circulation changes induced by tropical variability and Antarctic sea ice trends, and the work on the sea ice response to stratospheric ozone depletion has been inconclusive (e.g. Ferreira et al. 2015; Sigmond and Fyfe 2014; Kostov et al. 2016).

Some of the first coupled modeling studies to directly address the role of tropical teleconnections in Antarctic sea ice trends include Meehl et al. (2016) and Purich et al. (2016). Meehl et al. (2016) showed that Coupled Model Intercomparison Project, phase 5 (CMIP5) models consistently give positive Antarctic sea ice extent anomalies during the negative phase of the IPO, and that the few model runs which happen to show the negative phase IPO during 1999–2014 also show a positive Antarctic sea ice trend during that period, along with a deeper ASL. In contrast, during the full 1979–present period of the satellite sea ice record, the vast majority of model simulations show sea ice loss (e.g. Jones et al. 2016). This is consistent with the idea that natural variability, including that associated with the IPO, should dominate trends over the 15-year period of 1999–2014, while forced changes should be more evident in trends over the longer period of 1979–2014.

Purich et al. (2016) presented results from coupled model experiments in which observed three-dimensional ocean temperature and salinity anomalies were assimilated by the ocean model over various regions, including the global ocean as well just the equatorial Pacific. All of their data assimilation experiments showed ice loss over most regions of the Southern Ocean during 1979–2013. However, if the ensemble mean of the historical experiment is subtracted from the experiments with data assimilation, then the residual fields—which represent the influence of internal variability—show sea ice trend patterns that are more similar to the observed, especially in the global and tropical Pacific assimilation experiments. While suggestive of a role for the tropical Pacific in recent Antarctic sea ice trends, their results also indicate that the externally forced change may be too dominant in these experiments, since it had to be subtracted from the model results to obtain patterns similar to the observed.

The argument that observed Antarctic sea ice trends are consistent with natural variability has been made in part on the basis of large multi-model ensembles like the CMIP5 ensemble (e.g. Polvani and Smith 2013). Generally, the observed sea ice extent trend of approximately $+0.20 \times 10^6$ km^2/decade over the ~35 year record falls within the spread of ~35 year trends in pre-industrial control runs (Jones et al. 2016). However, if the spread of simulated historical trends during 1979–2005 is used in place of the pre-industrial trends, then the observed trend lies on the outer edge of the ensemble spread (Jones et al. 2016). Moreover, if information about the spatial and seasonal patterns of sea ice trends is used in the comparison of observations and models, then the observed trends in summer and autumn lie outside of the models' internal variability, and they are different from the models' forced response (Hobbs et al. 2015). The importance of using the historical trends, rather than the preindustrial trends, is that the simulated historical trends include the impacts of greenhouse gases and other anthropogenic forcings. Even if the observed Antarctic sea ice trend is consistent with natural variability, it has occurred in the context of externally forced climate change, and models should be able to account for natural and external factors simultaneously.

One problem with using the spread of multi-model ensembles such CMIP5 to study the role of internal variability is that the differences among simulated trends can arise from different model physics, in addition to internal variability. There are considerable differences in the climatology of Antarctica and the Southern Ocean among CMIP5 models, and there is evidence that these differences influence the simulated responses to external forcing. For instance, the present-day September SIE maximum ranges from about 4 to 23×10^6 km^2 among CMIP5 models (Zunz et al. 2013) and this range has a significant bearing on the simulated changes in twenty first century Antarctic sea ice, temperature and precipitation (Agosta et al. 2015; Bracegirdle et al. 2015). The wide range in sea ice climatology may relate to a similarly broad range in mean SST, which can be largely accounted for by differences in shortwave cloud forcing (Schneider and Reusch 2016). The response of clouds themselves to increasing greenhouse gases depends on their mean state and has large impacts on the resulting warming at the surface (Trenberth and Fasullo 2010; Gettleman et al. 2013; Tan et al. 2016), and by extension, on the amount of sea ice loss.

To overcome the often ambiguous meaning of differences within multi-model ensembles like CMIP5, we make use of a large, initial condition ensemble of a single model, the Community Earth System Model (CESM Large Ensemble, Kay et al. 2014). Each ensemble member is subject to the same forcing scenario, but starts from a slightly different atmospheric initial state. In this paper, the ensemble-mean of this "Large Ensemble" experiment is used to define the model's response to external forcing, while the ensemble spread is used to illustrate the role of internally generated variability on the simulated trends. As shown below, the observed Antarctic SIE trend during 1979–2013 lies outside the model spread. Observed tropical climate trends during this time period were unusually pronounced by some measures (e.g. England et al. 2014) and have contributed to the slowdown in global surface temperature trends (Kosaka and Xie 2013) as well as to atmospheric circulation trends over the Southern Ocean (Schneider et al. 2015). The chance that free-running historical climate model experiments simulate a sequence and magnitude of tropical variability like the observed is low.

The largest impacts of tropical variability, as well as the largest trends in Antarctic SIE, have occurred in the Pacific Sector of the Southern Ocean, which includes the Ross, Amundsen, and Bellingshausen Seas (e.g. Hobbs et al. 2016). The Ross Sea is the only region of the Southern Ocean where significant trends in SIE have occurred year-round (Hobbs et al. 2016). Figure 1 shows the timeseries of monthly sea ice extent anomalies in the Ross Sea, together with SST and wind anomalies across the Pacific Sector, and wind anomalies from the central equatorial Pacific. All timeseries exhibit a similar evolution of anomalies. The periods 1998–2002 and 2007–2014 for example are marked by positive sea ice extent anomalies, negative SST anomalies, westerly wind anomalies in the south Pacific and easterly wind anomalies in the central equatorial Pacific. Opposite-signed anomalies are present during 1991–1996 and 2002–2016. As noted above, the south Pacific wind anomalies were interpreted by Schneider et al. (2015) and linked with tropical teleconnections. The influence of large-scale atmospheric circulation variability in the Pacific Sector on Ross Sea SIE anomalies is discussed in Turner et al. (2016).

Given the potential importance of the evolution of tropical variability over the past several decades to Antarctic sea ice trends, it is perhaps not surprising that free-running coupled model experiments do not simulate the observed Antarctic sea ice trend. In addition to the 30-member Large Ensemble, we use a second initial condition ensemble of 10 members, in which the observed sequence of SST anomalies in the eastern tropical Pacific is specified using a nudging technique. The external forcings applied are the same as for the Large Ensemble. Trends in a given ensemble member of this experiment reflect a combination of the radiatively forced response, the response to tropical variability, and additional, internally-generated variability arising from atmosphere–ocean interaction or from intrinsic atmospheric and oceanic variability. The intention of this paper is to separate out these components in order to understand which one drives the overall trends in the model and in nature. As shown below, the response of sea ice to tropical variability is not enough to account for the gap between modeled and observed trends. The forced response of sea ice tends to dominate the modeled trends and is largely responsible for the observed-model mismatch. This leads us to suspect that the model's forced response is biased, and thus the final goal of this paper is to discuss some of the reasons for this bias.

The remainder of this paper is organized as follows. In Sect. 2, the model and the experiments are discussed in more detail, and the methods for defining the externally forced

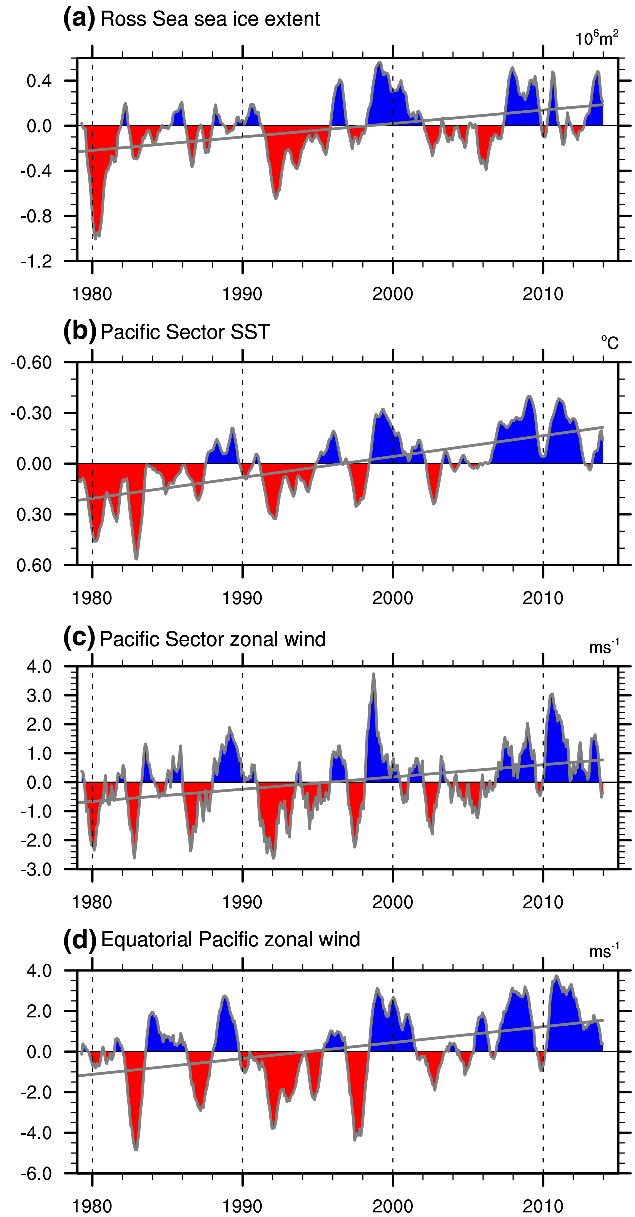

Fig. 1 Observed, monthly mean timeseries of anomalies in **a** Sea ice extent in the Ross Sea (160°E–130°W), **b** SST in the Pacific Sector (50°–70°S, 150°E–90°W), **c** zonal wind at 850 hPa in the Pacific Sector (40°–60°S, 70°–160°W) and **d** zonal wind at 850 hPa in the central equatorial Pacific (10°N–10°S, 160°E–160°W). For visual clarity, all timeseries are smoothed with an 8-month running mean and the common base period is 1981–2010. Note that the y-axis is reversed in **b** to highlight the similarity with the other timeseries

and tropically forced responses are explained. Section 3 gives the major results of the experiments, showing the externally forced and tropically forced patterns of trends in Antarctic sea ice and related variables in comparison with the observed patterns. The additional role of unforced internal variability, as given by the differences among individual ensemble members, is also highlighted. We discuss the

Table 1 Summary of the CESM1 experiments discussed in this paper

Experiment	Time-varying forcing	No. of runs
Large ensemble (LENS)	All radiative forcings	30
Tropical Pacific pacemaker (PACE)	All radiative forcings + Obs. SST anomalies (15°N–15°S; 80°–180°W)	10

Further details are given in Sect. 2.1 of the main text

physical processes that give rise to the sea ice trends, including anomalous ice motion, changes due to thermodynamics, and changes in the surrounding oceanic environment due to anomalous horizontal Ekman advection and air-sea heat fluxes. Section 4 discusses the implications of the results, especially in regards to possible model biases and provides summary and conclusion statements.

2 Materials and methods

2.1 Model and experiments

This study uses the fully coupled Community Earth System Model (CESM), version 1.1., configured with interactive atmosphere, ocean, land, and sea ice component models (e.g. Hurrell et al. 2013). The atmosphere and land are on a 0.9° latitude × 1.2° longitude horizontal grid and the sea ice and ocean are on a nominal 1° grid. This is a very stable and extensively evaluated configuration of the CESM, which has been used in a variety of climate science applications, including the experiments of the Coupled Model Intercomparison Project, Phase 5 (CMIP5, Taylor et al. 2012).

Results from two major CESM 1.1 experiments are analyzed (Table 1). The first experiment is the CESM Large Ensemble, or "LENS", a 30-member initial atmospheric condition ensemble designed for studying the impacts of climate change in the presence of internal variability. Details of this experiment are given in Kay et al. (2014). Most importantly, each ensemble member is forced in an identical way, except for an initial atmospheric temperature perturbation applied on the first day of the simulation. Due to the chaotic nature of the system, this small perturbation generates spread among the ensemble members. The second experiment is also an initial condition ensemble with random temperature perturbations applied at the start of each run. In addition, it follows the protocol of Kosaka and Xie (2013) in which the observed sequence of SST anomalies in the eastern tropical Pacific is specified using a nudging technique. In this experiment, SST anomalies in the eastern equatorial Pacific (15°N–15°S; 80°–180°W) from the

Extended Reconstruction SST version 3b dataset (ERSST v3b; Smith et al. 2008) are converted to sensible heat fluxes and applied to the ocean component model. A buffer zone of linearly tapering anomalies extends to 20°N and 20°S, and from 180°W to the coast of the Americas. The rest of the model's coupled climate system is free to evolve. Ten ensemble members of this "Pacemaker" experiment ("pacemaker" in the sense that the eastern tropical Pacific sets the 'pace' or sequencing of internal climate variability) were performed for the period 1920–2013. Note that our Pacemaker experiment (hereafter denoted "PACE") differs in several key ways from the temperature and salinity constrained pacemaker experiments discussed in Purich et al. (2016). First, the atmospheric model version used for PACE is CAM5 instead of CAM4 and the horizontal resolution of the atmosphere, ocean and land are ~1° instead of ~3.75°. Second, the most comparable experiment of Purich et al. (2016) is their Equatorial Pacific Ocean experiment, which assimilated anomalies over the entire tropical Pacific Ocean, rather than just the eastern equatorial Pacific. Finally, the Purich et al. (2016) experiments assimilated observed three-dimensional temperature and salinity anomalies into the ocean model, rather than just the SST anomalies.

All LENS and PACE ensemble members share the same external forcing, using the CMIP5 historical forcing specification for 1920–2005 and the RCP 8.5 forcing for 2006–2013 (details in Kay et al. 2014). The exception is that the LENS used stratospheric ozone concentrations from the whole atmosphere community climate model (WACCM), an interactive chemistry-climate model (Marsh et al. 2013), while the Pacemaker ensemble used stratospheric ozone concentrations from the SPARC dataset (Cionni et al. 2011), a dataset more commonly used in the CMIP5 historical experiments of other models. Schneider et al. (2015) compared atmospheric model experiments forced by SPARC and WACCM ozone, and found the lower tropospheric wind trends over the Southern Ocean for 1979–2011 to be statistically indistinguishable, with only subtle differences. The small difference in external forcing of the LENS and Pacemaker ensembles has minimal influence on the results discussed here.

For the analysis of sea ice trends, we take advantage of the model's ability to distinguish between sea ice area tendencies due to dynamics and tendencies due to thermodynamics. In the Community Ice Code version 4 (CICE4; Hunke and Lipscomb 2008; Holland et al. 2012), the sea ice model used in CESM1.1, the dynamic component of the model determines ice motion resulting from a force balance between wind stress, water stress, internal ice stress, and sea surface slope. The thermodynamic component of the model determines vertical and horizontal melt and growth rates by solving for the vertical temperature profile arising from the surface energy balance, vertical heat transfer, and heat supplied by the ocean at the bottom of the ice.

For comparison with the ensemble mean of the CESM1-LENS, we computed a multi-model ensemble mean from 29 models contributing to CMIP5. Monthly mean output was obtained from the first ensemble member of the 1850–2005 historical (twentieth century) experiment. The data were regridded to a common 1° latitude × 1° longitude grid. See Table S1 for a list of the models used.

2.2 Observational and atmospheric reanalysis datasets

To characterize the observed trends in sea ice and related variables, the following datasets are utilized: SST anomalies from ERSST v3b; sea ice concentration from the Goddard Merged analysis of passive microwave observations (Peng et al. 2013; Meier et al. 2013); oceanic potential temperature from the EN4 objective analysis, version 4.2.0 (Good et al. 2013); and geopotential height and zonal winds from the ERA-Interim Reanalysis (Dee et al. 2011).

2.3 Methods

The role of external radiative forcing, termed the "forced response", is obtained from the ensemble mean of the LENS experiment (denoted "LENS-EM"). The PACE ensemble mean (denoted "PACE-EM") includes both the forced response and the response to observed internal tropical variability. The role of the tropics (specifically, the eastern Equatorial Pacific), called the "tropical response", is isolated by subtracting LENS-EM from PACE-EM. Individual ensemble members of PACE reflect a combination of the forced response, the tropical response, and internal variability beyond the eastern Equatorial Pacific. The goal of these methods is to separate out these three components, as summarized in Table 2. Nature should be most comparable with an individual ensemble member, rather than any one component. The estimate of the tropical response assumes that the responses to tropical SSTs and external forcings are linear. This assumption may not strictly hold, and in any event, it is difficult to purely separate external and tropical signals, as the observed tropical SSTs themselves have been influenced by external forcing. This caveat notwithstanding, the results here are consistent with the expected response to recent tropical variability, namely a deepened ASL and lower SSTs and expanded sea ice in some sectors of the Southern Ocean.

The sea ice extent (SIE) is defined as the total area of grid cells containing an ice fraction of 15% or greater. For observations, we calculate extent from the polar stereographic grids of the Goddard Merged data, using cell areas provided by the National Snow and Ice Data Center. For the models,

Table 2 Summary of how the role of various drivers is determined

Response	How derived	SIE trend ($\times10^6$ km^2/decade)
Radiatively forced response	LENS-EM	−0.45
Tropical response	LENS-EM minus PACE-EM	0.09
Tropical response + intrinsic variability	PACE #4 minus LENS-EM	0.18

Further details are given in Sect. 2.2 of the main text

we calculate SIE from the atmospheric grid, using cell areas provided by the CESM modeling group.

We also use output from the ocean model to compute the horizontal Ekman heat flux and the air-sea heat fluxes. The Ekman term is computed on the ocean grid, applying the surface stress to the horizontal temperature gradients in the uppermost ocean layer. The surface heat flux term, Q_{net}, is also computed on the ocean grid. Q_{net} includes the ocean heat flux due to ice formation or ice melting, the sensible and latent turbulent heat fluxes, and the net surface longwave and net surface shortwave radiative fluxes, all as viewed from the ocean's perspective.

Monthly anomalies in all variables are computed by subtracting the climatological monthly means for the base period of 1981–2000 from the corresponding month of each year. Seasonal averages are formed from the monthly anomalies and referred to by the first letters of the corresponding month means (e.g. August–September–October is ASO). Linear least-squares analysis is used to compute trends. Stippling is used on the plots to indicate areas of statistical significance, which is determined from a two-sided *t* test methodology and adjustment for autocorrelation as outlined by Santer et al. (2000). Unless otherwise noted, the sample size and the degrees of freedom for indexing the critical *t* value are adjusted according to the lag-1 autocorrelation of the residuals.

3 Results

3.1 Observed and simulated monthly trends in atmospheric circulation and sea ice

We begin by describing the hemispheric-scale context in which the Antarctic sea ice increase has occurred. Observed 850-hPa geopotential height trends during 1979–2013 based on all months of the year (Fig. 2a) exhibit a wave-train pattern in the Southern Hemisphere (SH), with positive height trends in the south Pacific Ocean centered near 100°W, negative height trends off the coast of Antarctica centered near 80°W and positive height trends in the south Atlantic Ocean centered near 60°W. The negative height trends near Antarctica are a signature of a deepened Amundsen Sea Low (ASL, e.g. Raphael et al. 2016). The pattern of negative SST trends in the eastern Pacific basin of both hemispheres, contrasted with positive SST trends in the western Pacific, resembles the negative phase of the PDO (e.g. Trenberth et al. 2014). SST cooling is largest in the Pacific Sector of the Southern Ocean. As the highly correlated timeseries in Fig. 1 suggest and the work of Yeo and Kim (2015) shows, the SST cooling is physically consistent with the overlying atmospheric circulation trends.

Figure 2b,c depict analogous height and SST trends from the model experiments. The forced response, given by LENS-EM (Fig. 2b) shows positive SST trends nearly everywhere, except for a small region in the north Atlantic. The warming is largest in the polar regions of both hemispheres (note that the model's SST shown in this figure is the surface skin temperature, which responds strongly to changes in sea ice cover, and is not directly comparable to the observed SST in the ice-covered regions). Over the tropical and mid-latitude oceans, the forced response of SST shows little spatial structure, with subtle regional patterns including a maximum of warming along the equatorial Pacific, which has been associated with wind anomalies (Xie et al. 2010). The most notable geopotential height trend in the forced response is a weak expression of the positive SAM pattern, marked by negative trends polewards of 60°S, and positive trends in the SH midlatitudes. The forced response given by LENS-EM is similar in many respects to that given by the multi-model mean of CMIP5 (Fig. S1), suggesting that the CESM1 is not an outlier with respect to its forced response. In SST, LENS-EM and CMIP5-EM show the strongest warming at the poles and a local maximum of warming in the equatorial Pacific. Like the LENS-EM, the CMIP5-EM shows a weakly positive SAM pattern in its geopotential height trend, although the node is shifted somewhat equatorward in CMIP5-EM compared with LENS-EM.

PACE-EM (Fig. 2c) shows the dramatic effect of specifying the observed tropical Pacific SST variability in addition to external forcing. Cooling is evident in the eastern Pacific basin of both hemispheres, while the Southern Ocean near West Antarctica warms considerably less than in LENS-EM. A wave-train pattern in 850-hPA height trends in the SH, similar in form but weaker in magnitude to the observed, is also evident in PACE-EM. Differencing the PACE-EM and

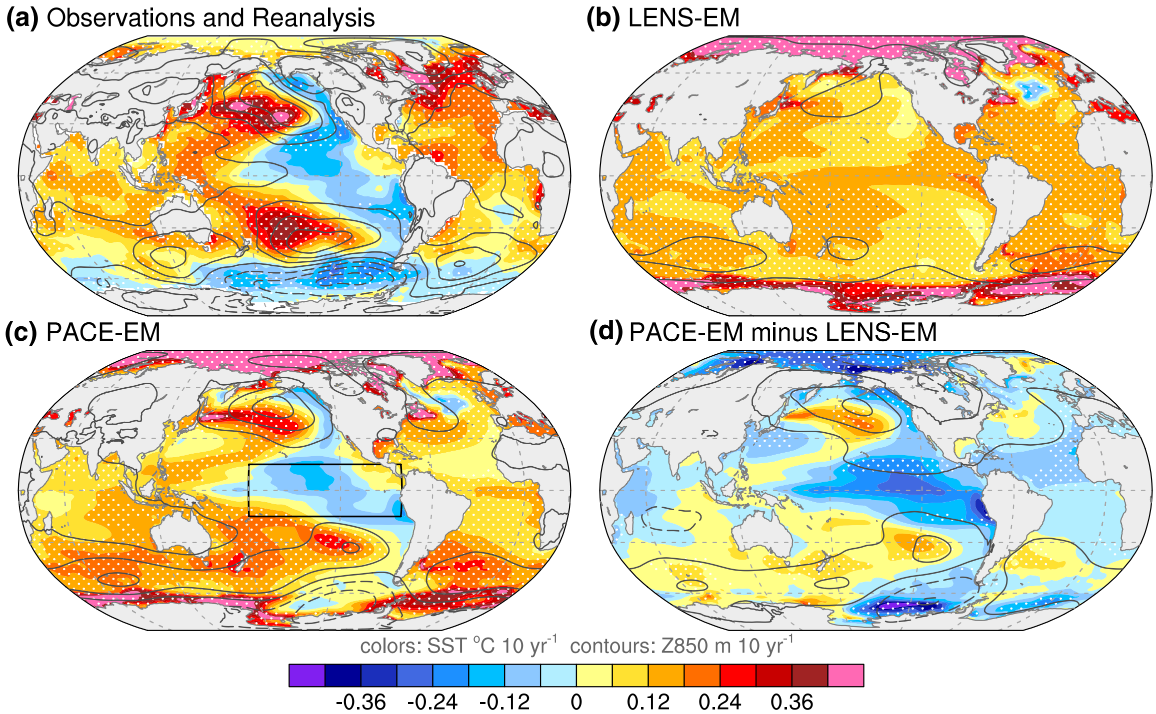

Fig. 2 Trends in SST (*colors*) and 850 hPa geopotential height (contours, spacing of 2 m/decade, negative trends *dashed lines* and positive trends *solid lines*) over 1979–2013, using all months, for **a** observations and reanalysis, **b** the ensemble mean of the LENS, **c** the ensemble mean of PACE, **d** the difference of the ensemble means of LENS and PACE. *Stippling* indicates that the local SST trend is significant at or above the 90% level

LENS-EM patterns isolates the tropical response (Fig. 2d), which shows cooling over most of the global ocean, especially in the eastern Pacific basin and the Pacific and Atlantic sectors of the Southern Ocean. The tropical response largely accounts for the wave-train pattern in SH geopotential height trends that is evident in PACE-EM.

The corresponding Antarctic sea ice concentration (SIC) trends are displayed in Fig. 3a–d. In observations (Fig. 3a), SIC trends are positive in most regions, except for the Bellingshausen Sea near the Antarctic Peninsula and the Amundsen Sea near coastal West Antarctica. By contrast, the forced response (Fig. 3b) is characterized by sea ice loss nearly everywhere, especially at the northern ice edge. This pattern is largely mirrored in PACE-EM (Fig. 3c) except in the Pacific sector, where SIC trends are very weak. The tropical response (Fig. 3d), therefore, is associated with a modest but statistically significant ice gain in the Pacific sector and is notable for the lack of negative SIC trends in most regions of the Southern Ocean. We shall describe the remaining panels of Fig. 3 below.

To quantify the observed and modeled SIE trends, Fig. 4 shows the Antarctic SIE trend over 1979–2013 in each ensemble member, the observations, and the ensemble means, including the multi-model ensemble mean, CMIP5-EM. In contrast to the observed trend of $+0.20 \times 10^6$ km^2/decade, the forced response from LENS-EM is -0.45×10^6 km^2/decade, only slightly more negative than CMIP5-EM, while PACE-EM is -0.36×10^6 km^2/decade. Differencing LENS-EM and PACE-EM yields the tropical response of $+0.09 \times 10^6$ km^2/decade. The role of internally generated variability is illustrated by the ensemble spreads. In the LENS, the simulated trends range from -0.74×10^6 to -0.12×10^6 km^2/decade and in PACE, the simulated trends range from -0.50×10^6 to -0.27×10^6 km^2/decade. This suggests that internal variability, superimposed on the forced or the forced plus tropical responses, does not account for the sign and magnitude of the observed Antarctic sea ice trend. However, if the forced response is subtracted out of each ensemble member, then the ensemble spreads of the residual LENS and Pacemaker ensembles overlap the observed trend. When the forced response is removed, nine out of ten PACE ensemble members show positive SIE trends. The largest trend, $+0.18 \times 10^6$ km^2/decade—close to the observed value—is in ensemble member four (PACE #4); this ensemble member is analyzed further below.

In map view (Fig. 3e), the original PACE #4 shows SIC trends with a pattern similar to PACE-EM (Fig. 3c), but of larger magnitude. Removing the forced response results in positive SIC trends in most regions of the Southern Ocean (Fig. 3f), especially in the Amundsen and eastern Ross seas.

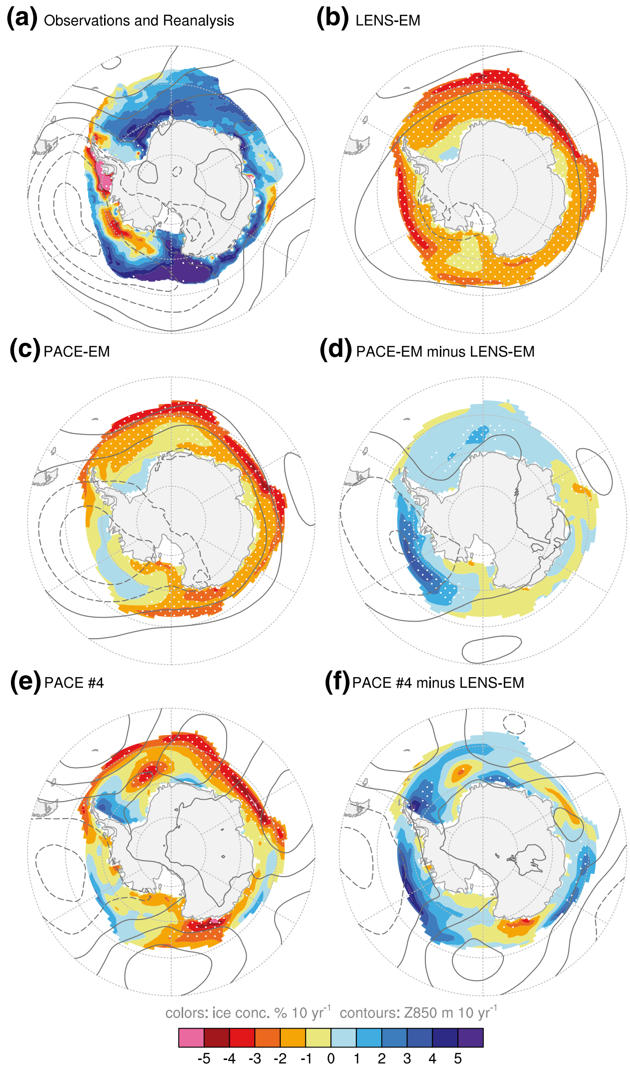

Fig. 3 Trends in sea ice concentration (*colors*) and 850 hPa geopotential height (contours, spacing of 2 m/decade, negative trends *dashed lines* and positive trends *solid lines*) over 1979–2013, using all months, for **a** observations and reanalysis, **b** the ensemble mean of the LENS, **c** the ensemble mean of PACE, **d** the difference of the ensemble means of LENS and PACE, **e** PACE #4, and **f** the difference of PACE #4 and the ensemble mean of the LENS experiment. *Stippling* indicates that the local sea ice concentration trend is significant at or above the 90% level

This "residual pattern" may be interpreted as the trend arising from a combination of the tropical response (Fig. 3d) plus intrinsic variability beyond the tropical Pacific. In PACE #4, the intrinsic variability generally acts to reinforce the pattern associated with the tropical response.

Timeseries of Antarctic SIE from the experiments and observations (Fig. 5a) emphasize the systematic nature of the forced response and the data-model mismatch that has received much attention. All ensemble members of both the LENS and PACE experiments exhibit negative trends during 1979–2013, consistent with Fig. 4. The trends during this period are part of a longer-term decline in SIE that is evident when the timeseries are extended about a decade before and after the 1979–2013 observational period. This long-term, gradual decline in ice cover is consistent with the external forcing (mainly, rising greenhouse gas concentrations) applied to the model. The LENS-EM and CMIP5-EM timeseries behave similarly, suggesting that CESM1 agrees with the multi-model consensus of the forced response. With the forced response retained in the PACE experiment, the observed timeseries falls outside the bounds of the ensemble. With the forced response removed, however, the observed timeseries lies within the ensemble (Fig. 5b). The timeseries of the tropical response (purple line, Fig. 5b) shows a modest positive trend that results from predominantly negative anomalies before the late 1990s and predominantly positive anomalies after the late 1990s.

3.2 Seasonal-mean responses in sea ice and atmospheric circulation

Having considered the large-scale, all-month trends in sea ice and related variables, we now turn to seasonal-mean trend patterns. The seasons are delineated to capture the late winter sea ice maximum extent (ASO), the rapid retreat in spring and summer (NDJ), and the gradual ice advance in autumn and winter (FMA and MJJ). In observations (Fig. 6a), ice gain during 1979–2013 occurs in all seasons. In the winter (ASO and MJJ), the largest gains in SIC are at the ice edge, while in summer and autumn, the largest gains are closer to the continent, and are especially pronounced in the western Ross and eastern Weddell seas. Ice loss occurs near the Antarctic Peninsula in all seasons, and along coastal West Antarctica in the summer and autumn. The modeled SIC trend patterns are quite different from the observed. The forced response (Fig. 6b) exhibits ice loss in all seasons, mainly at the ice edge during winter and near the coast in autumn, with relatively little change in summer. The tropical response (Fig. 6c) shows ice gain in all seasons, with the largest magnitudes in ASO in the Pacific sector.

In the overlying atmospheric circulation trends, the forced response (Fig. 6b) has the largest magnitude in summer, in the form of the positive SAM pattern, with negative height trends over Antarctica and positive trends over the mid-latitudes. The tropical response (Fig. 6c) is associated with negative height trends in the Pacific sector in all seasons, most spatially extensive during the winter. In ASO, positive height trends occur in the Eastern Hemisphere, giving shape to an east–west dipole that broadly resembles the observed pattern.

Given that the tropical response shows the largest SIC trends in ASO and the overlying atmospheric circulation pattern resembles the observed pattern, we focus on ASO for further analysis. Figure 7 repeats the layout of Fig. 3,

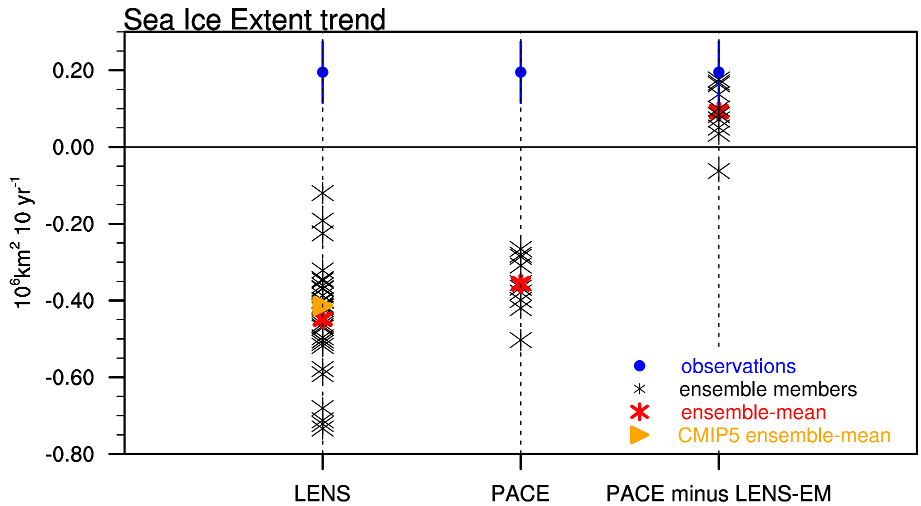

Fig. 4 Antarctic sea ice extent trends, using all months during 1979–2013, as given by the observations, the LENS, the PACE, and the difference of the PACE and the LENS ensemble-means. The 95% confidence bound of he observed trend is given by the *solid blue line*. Also indicated is the trend in the CMIP5 ensemble mean for 1979–2005

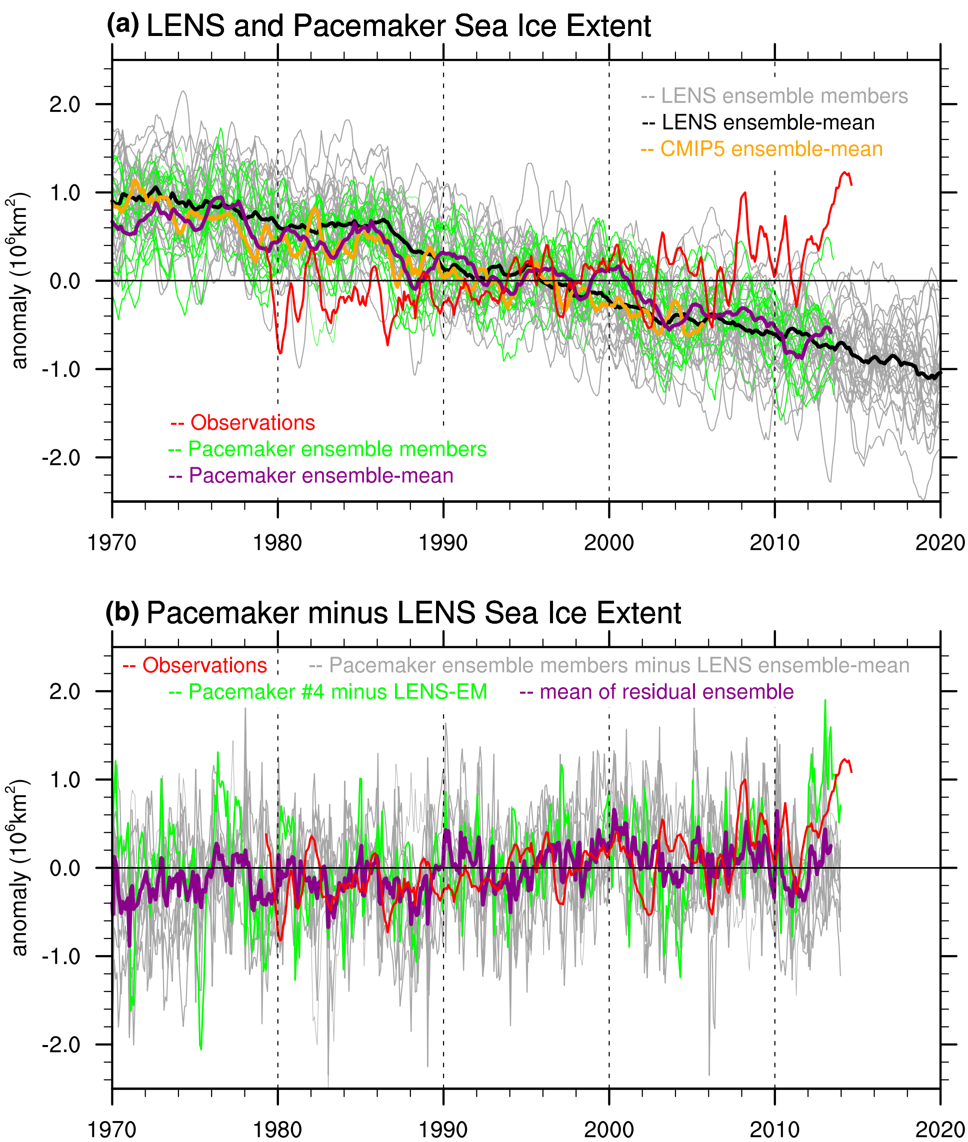

Fig. 5 Timeseries of anomalies in Antarctic sea ice extent, using all months, according to **a** the LENS and PACE and **b** the residual of the PACE runs minus the ensemble mean of the LENS experiment. The observed timeseries is shown in both *panels*, and the CMIP5 ensemble mean is shown in **a**. For visual clarity, the original timeseries are smoothed with a 10-month running mean and the common base period is 1981–2010

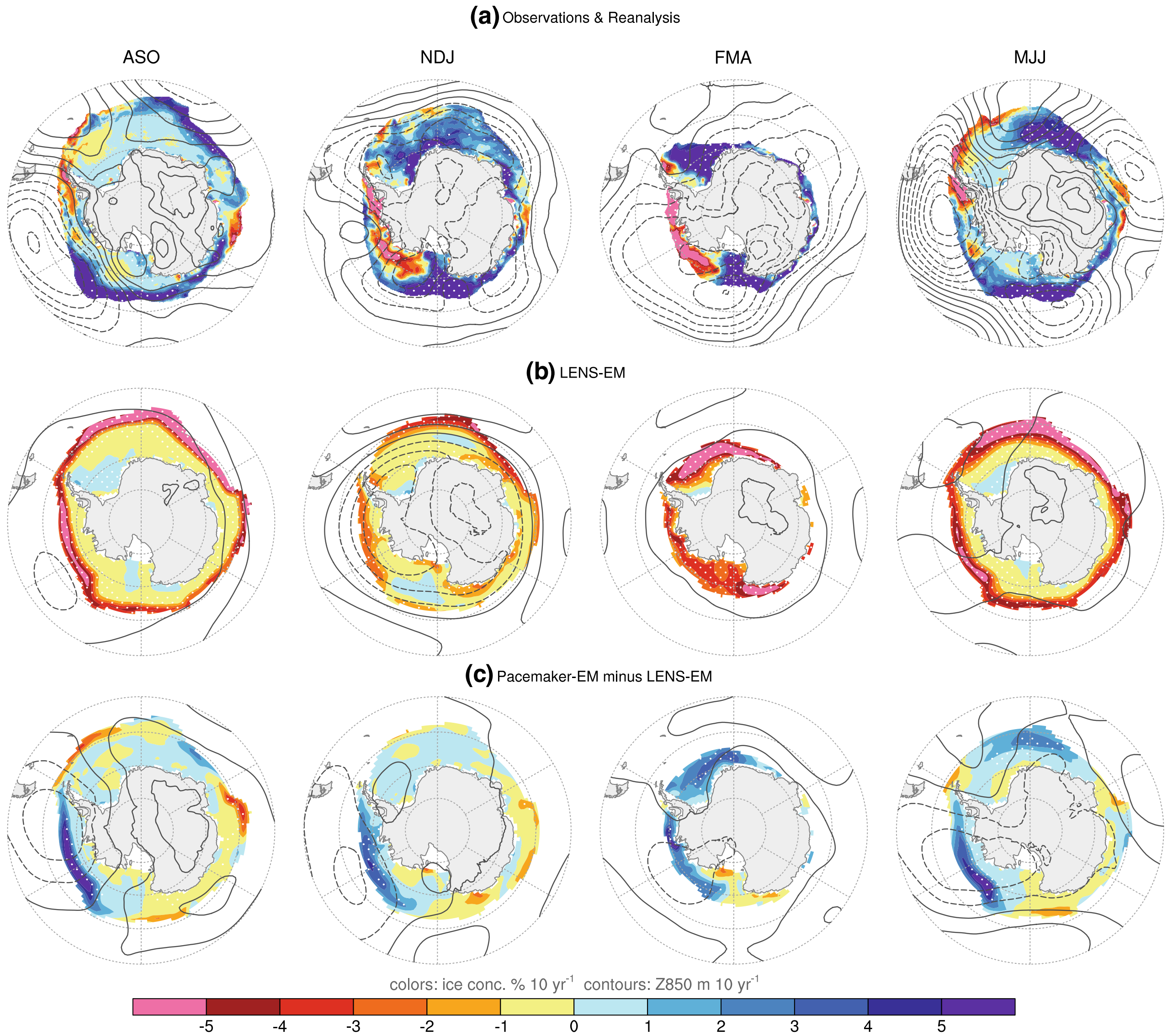

Fig. 6 Trends in seasonal-mean ice concentration (*colors*) and 850 hPa geopotential height (contours, spacing of 2 m/decade, negative trends *dashed lines* and positive trends *solid lines*) over 1979–2013, for **a** observations and reanalysis, **b** the ensemble mean of the LENS, and **c** the difference of the ensemble means of LENS and PACE. *Stippling* indicates that the local sea ice concentration trend is significant at or above the 90% level

but for ASO instead of the monthly means. The atmospheric circulation trend in PACE #4 (Fig. 7e) is similar to the observed (Fig. 7a), both in terms of the east–west dipole in the sign of the trend, and in terms of the position and magnitude of the maximum low pressure trend near 56°S, 110°W. Despite the realistic pattern and magnitude of the atmospheric circulation trend, the SIC trend pattern in PACE #4 does not resemble the observed, with the notable exception that the dipole in the sign of the trend is present between the Peninsula region and the eastern Ross Sea. Subtracting out the forced response (Fig. 7f) has little influence on the atmospheric circulation trend, but yields a SIC trend pattern that is comparable in sign and magnitude to the observations. In the Amundsen and eastern Ross Sea (90°–160°W; blue box in Fig. 7e), where the simulated positive SIC trends are largest, increasing SIC is associated with anomalous northward and westward ice motion. This pattern of ice motion trends is consistent with expectations from observations, in that freely drifting ice moves at a small angle to the left of the geostrophic winds, which are parallel to the geopotential height contours (e.g. Holland and Kwok 2012; Kimura et al. 2004). In addition, as discussed by Fan et al. (2014), Raphael et al. (2016) and others, cold air advection associated with northward geostrophic wind anomalies in the eastern Ross Sea also leads to increased SIC and extent.

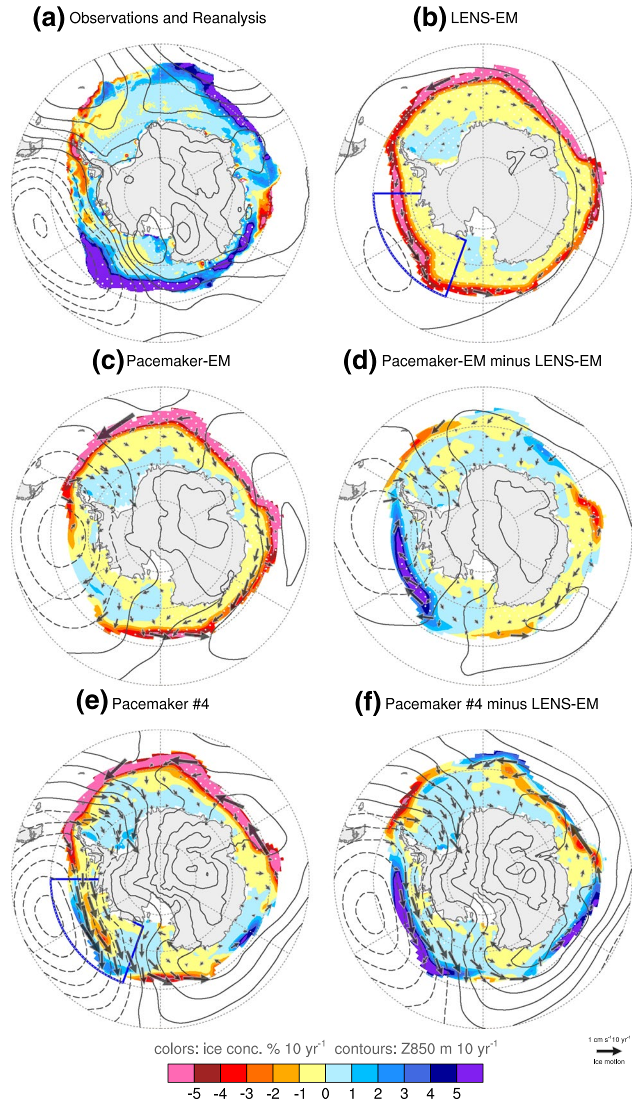

Fig. 7 Same layout as Fig. 3, but for ASO and also including the trends in ice motion shown as *arrows*. *Stippling* indicates that the local sea ice concentration trend is significant at or above the 90% level

3.3 Dynamic and thermodynamic aspects of the sea ice response

Next we further examine the physical mechanisms of the sea ice responses, using the dynamic and thermodynamic sea ice area tendencies given by the CICE model. To provide context to the changes in these terms, Fig. 8 displays the climatology from the LENS ensemble mean. In general, thermodynamic and dynamic processes offset each other. Near the continent, the climatological mean ice motion is divergent (Fig. 8a) and the dynamic ice area tendency is negative (Fig. 8b). This creates openings for new sea ice to form in the cold polar waters, so the thermodynamic tendency is positive (Fig. 8c). Near the ice edge, the ocean is too warm to support thermodynamic ice growth, but the ice motion is convergent and the dynamic tendency is positive. Within a relatively small band as the winter ice edge is approached, the ice concentration drops rapidly from 80% to less than 20% (Fig. 8a) and the interannual standard deviation of ice concentration is large (Fig. 8d). It is changes within this "marginal ice zone" that are most reflected in SIE anomalies.

We now consider the thermodynamic and dynamic tendencies in the region of the Amundsen and eastern Ross Sea where the SIC increases the most in the tropical response and in the residual (blue-outlined area in Fig. 7e). From south to north, the climatological ice concentration decreases from 100% at 72°S, to 15% (the conventional ice edge) at about 62°S (Fig. 9a). At approximately 66°S, the ice motion changes from divergent to convergent, and the thermodynamic tendency changes from positive to negative. The relatively sparse ice cover equatorwards of 66°S is maintained by dynamics, with the ice moving in a northward and eastward direction.

Changes in these terms in the LENS and PACE experiments during 1979–2013 are shown in Fig. 9b, using an epoch difference (1999:2013 minus 1979–1998) to enable direct comparison to the mean state (trend results are similar; not shown). The forced response (black line in Fig. 9b) is characterized by maximum ice loss at 66°S. This change implies a small poleward shift in the latitude at which the sea ice is thermodynamically stable. The dynamic changes are too weak in the forced response to offset the ice lost due to thermodynamics. In the tropical response (dashed blue line in Fig. 9b), ice gain at 66°S corresponds with weak thermodynamic ice growth, which is enabled by enhanced divergent ice motion. Equatorwards of 66°S, the gain in ice concentration is supported by dynamics, which is reflected in the increased northward and eastward ice motion. In the residual pattern (PACE #4—LENS-EM; red line in Fig. 9b), ice gain is maximized between 66° and 62°S, associated with positive tendencies due to thermodynamics between 66° and 64°S and due to dynamics between 64°S and 62°S. The positive thermodynamic ice tendency around 66°S may be viewed as a response to the divergent ice motion. Equatorwards of where the ice motion change switches to convergent at 64°S, dynamics help to increase the ice cover. At about 62°–63°S, the northward component of the ice motion more than doubles compared to the climatology (the climatology is ~0.4 cm/s, which increases by ~0.5 cm/s), acting to expand the ice edge.

3.4 Associated changes in SSTs and air-sea heat fluxes

As discussed by Armour and Bitz (2015) and Fan et al. (2014), the observed Antarctic sea ice increase should be viewed in the context of SST trends across the entire Southern Ocean. To understand the context in which the

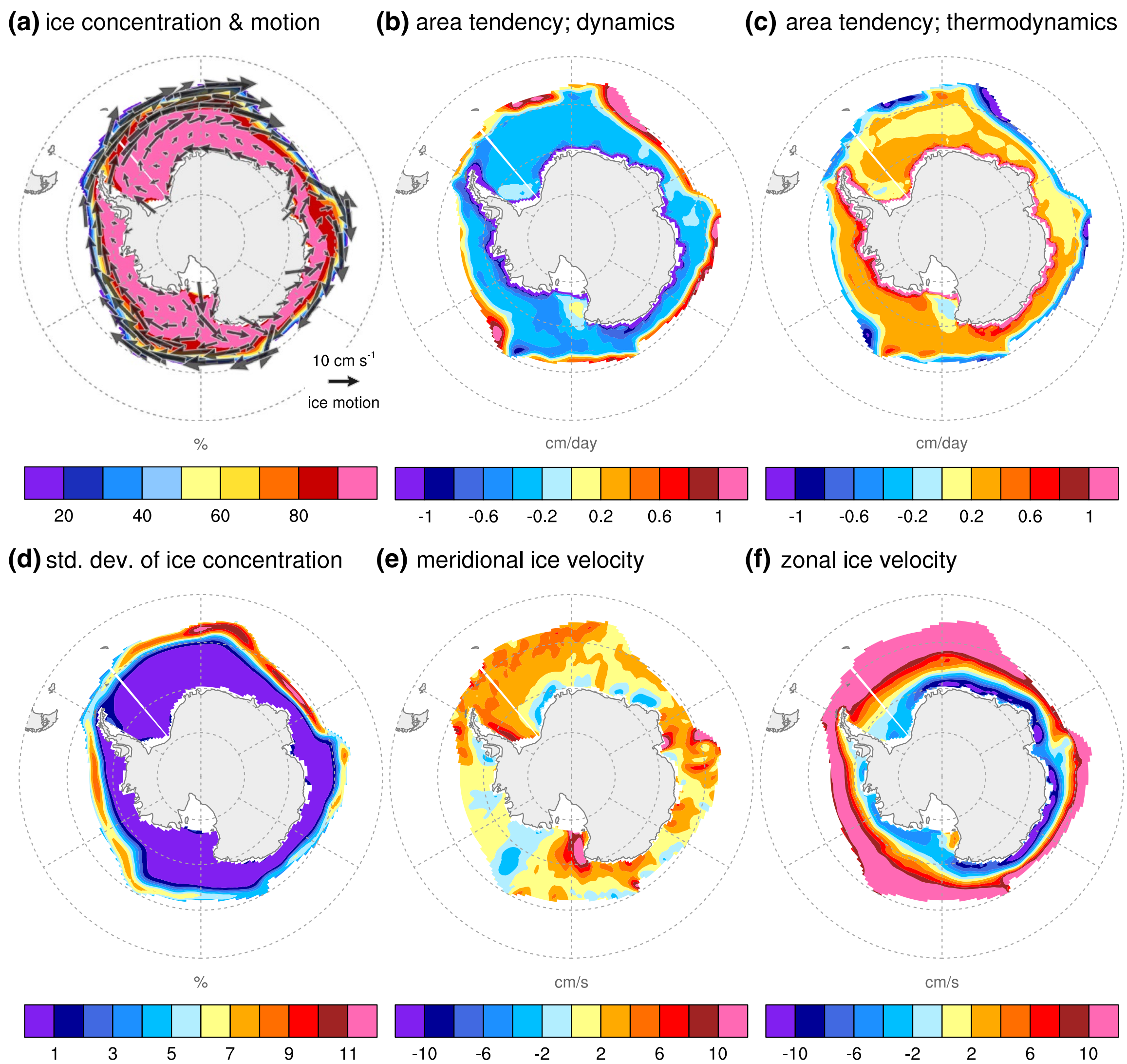

Fig. 8 Seasonal climatology for ASO according the ensemble mean of the LENS experiment of **a** ice concentration and motion, **b** ice area tendency due to dynamics, **c** ice area tendency due to thermodynamics, **d** interannual standard deviation of ice concentration, **e** meridional component of ice motion and **f** zonal component of ice motion

sea ice changes discussed above occur in the model environment, we compute the trends in horizontal Ekman heat flux and air-sea heat fluxes and compare these patterns to the SST trends for the region 30°S to the Antarctic coast.

In the forced response (Fig. 10a), the SST increases everywhere. The Ekman heat flux is predominantly negative, consistent with the largely westerly wind forcing, which can be inferred from the geopotential height patterns in Fig. 6b. The surface heat flux pattern largely reflects changes at the retreating ice edge, as heat is removed from the ocean where ice is lost and added to the ocean equatorwards of the ice edge. The relatively weak atmospheric circulation changes in the forced response are likely not a strong driver of the heat flux trends.

In the tropical response (Fig. 10b), the SST and Ekman trends are zonally asymmetric and show a broad-scale correspondence to each other. These patterns are consistent with the east–west dipole in the atmospheric circulation trend discussed above (e.g., Fig. 6b). The Q_{net} term is less influenced by the ice edge than in the forced response, except in the south Pacific sector, where ice gain is associated with reduced heat loss. Generally, the combined Ekman and surface heat fluxes help to drive the SST pattern rather than damp it (that is, the heat flux and SST trends are of the same sign in most regions).

The SST and Ekman patterns in the residual pattern (Fig. 11b) resemble those in the tropical response, but they are stronger in magnitude, consistent with the relatively

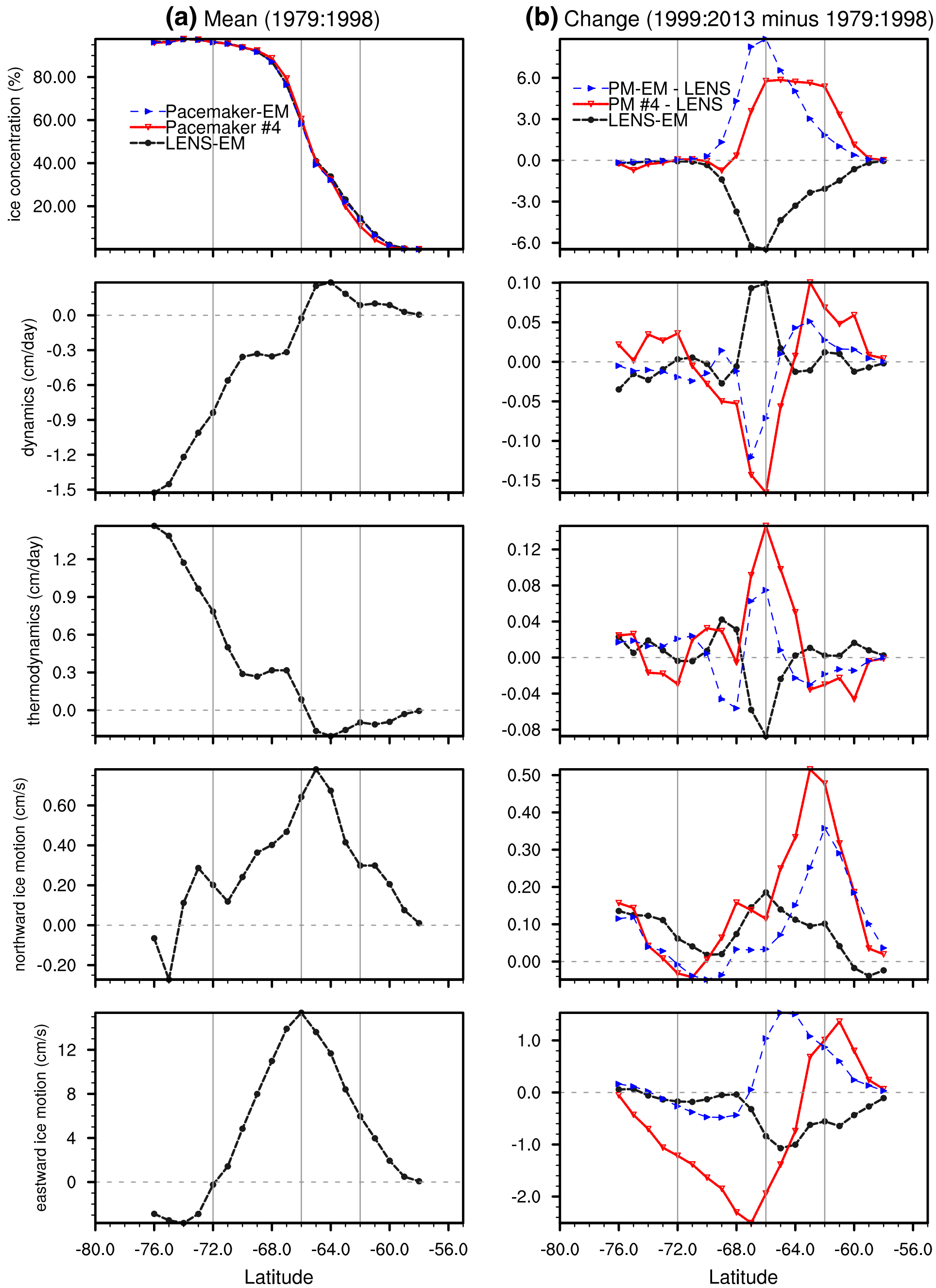

Fig. 9 Latitudinal transects integrated over the eastern Ross Sea and Amundsen Sea region (90°–160°W) of, from *top* to *bottom row*, ice concentration, ice area tendency due to dynamics, ice area tendency due to thermodynamics, meridional ice motion and zonal ice motion. *Column* **a** shows the mean over 1979–1998 and *column* **b** shows the differences of the means between 1999 and 2013 and 1979–1998

strong atmospheric circulation trends (see Fig. 7f). The Q_{net} term is much stronger than in the ensemble means, consistent with the stronger atmospheric circulation trends and associated changes in wind speed, meridional heat advection, cloud cover and precipitation. Broadly, the combined Ekman and surface heat fluxes are of the same sign as the SST trends. Importantly, the negative heat flux and SST trends in the south Pacific sector help to support the ice expansion there, reinforcing the trends associated with enhanced ice motion. Similarly, positive heat flux trends are co-located with reduced ice extent in the western Weddell Sea region, reinforcing the anomalous poleward ice motion. The observed SST trend (Fig. 11a) more closely resembles the residual pattern than it does the forced response. The model results suggest that both Ekman and surface air-sea heat fluxes have contributed to the negative SST trends in Pacific Sector.

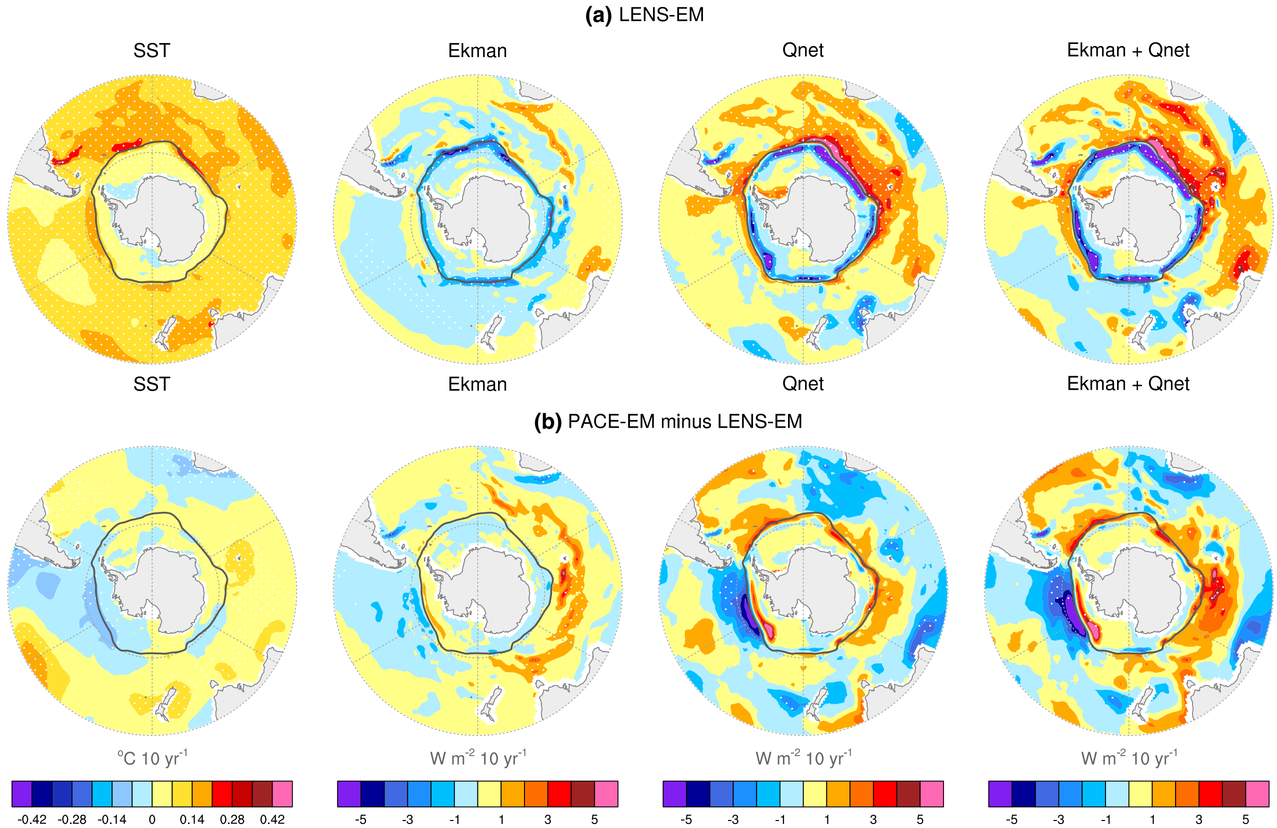

Fig. 10 Trends in the ASO seasonal-mean, from *left* to *right column*, SST, Ekman heat flux, surface heat fluxes, and the sum of the Ekman and surface heat fluxes during 1979–2013 for **a** the ensemble mean of the LENS and **b** the ensemble mean of PACE minus the ensemble mean of LENS. Also indicated in *each panel* is the ASO ice edge, shown as the *solid black line*. *Stippling* indicates that the local SST or heat flux trend is significant at or above the 90% level

4 Discussion

The above results add to the body of work that highlights the observed-model discrepancies in recent Antarctic sea ice trends (e.g. Turner et al. 2013; Zunz et al. 2013; Hobbs et al. 2015; Jones et al. 2016). Using a large ensemble of historical simulations with the CESM, we have examined the role of internal variability in explaining this discrepancy. This expands previous work using multi-model ensembles (e.g. Polvani and Smith 2013; Jones et al. 2016) in which it is difficult to disentangle the roles of structural uncertainty and internal variability. Given that all ensemble members of the LENS show a decrease in Antarctic sea ice extent during 1979–2013, in contrast to the observed increase, it seems that internal variability alone is an insufficient explanation for the observed-model mismatch. With a second ensemble of the CESM, we have considered the hypothesis that SST variability in the tropical Pacific has been a driver of Antarctic sea ice trends (e.g. Meehl et al. 2016; Purich et al. 2016). This Pacemaker experiment supports this hypothesis by showing less sea ice loss compared to the LENS, especially in the Pacific Sector. In addition, the Pacemaker experiment reproduces the dominant spatial pattern of atmospheric circulation trends in the mid-to-high-latitude SH, most importantly a deepened ASL. However, despite giving realistic atmospheric circulation trends over the Southern Ocean, none of the pacemaker ensemble members simulates a positive trend in Antarctic sea ice extent over 1979–2013. By including the observed sequence of tropical variability and thereby more realistically capturing circulation trends over the Southern Ocean, the pacemaker simulations reduce the possibility that data-model discrepancies in sea ice trends result from an unusual sequence of internal variability.

The ensemble-mean of the LENS experiments provides a good estimate of the radiatively forced response of sea ice and related variables, and it is in broad agreement with the multi-model mean from CMIP5. In CESM, as in most models (e.g. Hobbs et al. 2016), the forced sea ice trend differs sharply in sign and spatial pattern from the observed trends. In all seasons of the year, the forced response shows sea ice loss in every sector of the Southern Ocean (e.g. Fig. 6b). Typically, in comparing observed and modeled trends, we would expect nature to more closely resemble a single ensemble member than the forced response. However, in

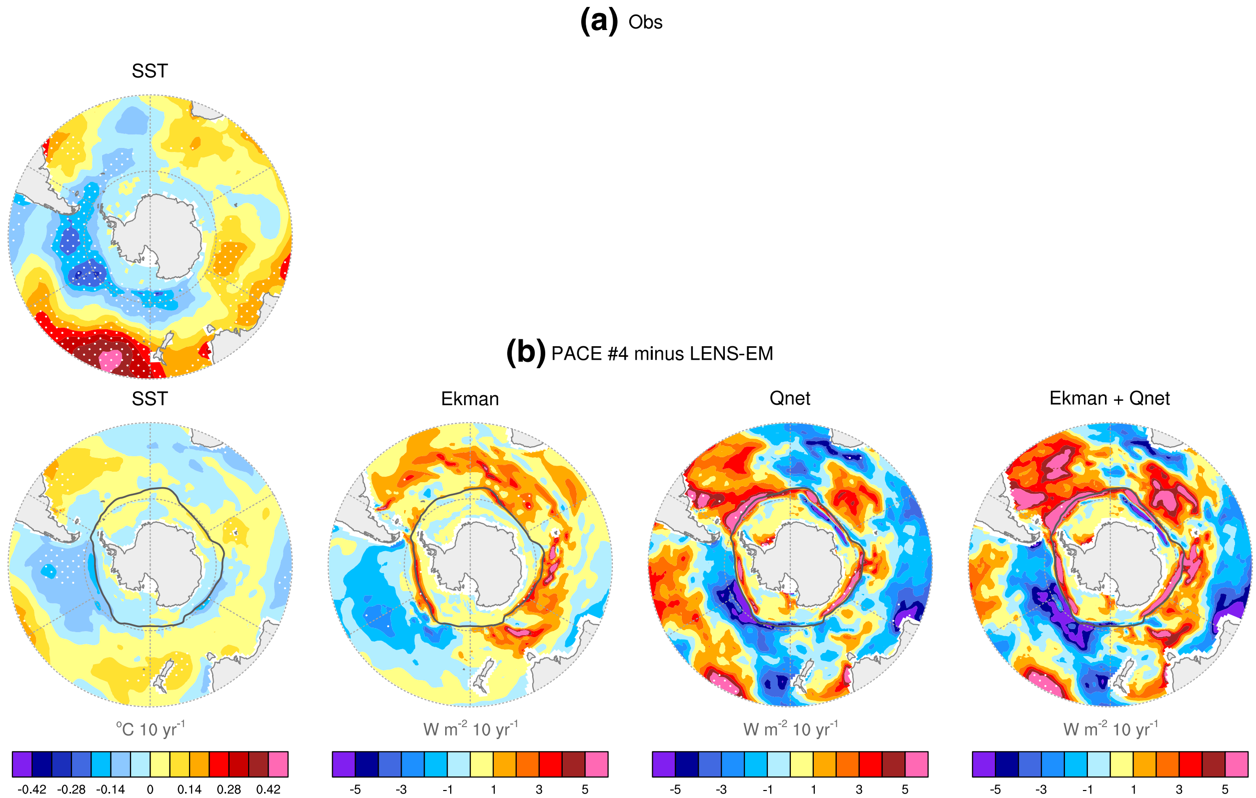

Fig. 11 **a** Trend in the ASO seasonal-mean SST according to observations during 1979–2013. **b** As in Fig. 10, but for the difference of the PACE #4 and the ensemble mean of the LENS. *Stippling* indicates that the local SST or heat flux trend is significant at or above the 90% level

the case of Antarctic sea ice, the forced response dominates the trends in every ensemble member, so that none of the ensemble members look like nature. This leads us to suspect that the Antarctic sea ice in the model is too sensitive to external forcing. Support for this conclusion is provided by the fact that if the forced response is subtracted out of each ensemble member, then the observed sea ice trend falls within the ensemble spread of both the LENS and pacemaker ensembles.

Removing the forced response and accounting for the influence of tropical teleconnections are two important factors in resolving the observed-model discrepancies in Antarctic sea ice trends. The impacts of these two steps are illustrated by comparing the forced response (e.g. Fig. 3b) with the tropical response (e.g. Fig. 3d). The latter shows a net increase in Antarctic sea ice extent with the greatest gains in ice concentration in the Pacific sector, underlying a deepened ASL. The tropical response pattern is similar to the results of the equatorial Pacific data assimilation experiment of Purich et al. (2016) (see their Fig. 2d). However, an additional role is played by internal variability associated neither with external forcing nor tropical teleconnections. Such intrinsic variability can strongly impact decadal-scale atmospheric circulation trends as well as the underlying sea ice trends, as illustrated by sea ice simulations forced by synoptic-scale atmospheric variability (Matear et al. 2015). We examine the role of intrinsic variability by removing the forced response from the individual ensemble members of the PACE experiment. In one member (PACE #4), this doubles the overall sea ice extent trend that can be explained compared to the ensemble-mean of PACE (e.g. Fig. 4). In PACE #4, the atmospheric circulation trends and sea ice trends in austral winter are similar to the observed (e.g. Fig. 7f, a). In summary, if we hypothesize that the radiatively forced response is flawed (in the sense that it is too strong, of the wrong sign, or incorrect spatial pattern) and that internal variability (including that arising from tropical teleconnections and extratropical atmosphere-ocean-sea ice dynamics) plays an important role, we can then largely explain the observed-model discrepancy in Antarctic sea ice trends.

The austral winter sea ice grain in the residual pattern (PACE #4 minus LENS ensemble-mean) occurs for reasons physically consistent with expectations from observations. In the model, the sea ice gain in the Amundsen and eastern Ross Sea is associated with an increase in ice motion driven by an intensified ASL. In the region of ice divergence (polewards of ~64°S), thermodynamic ice growth replaces the ice cover exported from the region, leading to a net increase in ice concentration. Equatorwards of ~64°S, a strong increase in northward and eastward ice motion helps to expand the sea ice extent. Holland and Kwok (2012) described a similar scenario for the observed autumn and winter Antarctic sea ice expansion during 1992–2010, lending observational support to the mechanisms of sea ice expansion in the model. In the model and in nature, the sea ice expansion is likely enhanced by feedbacks associated with the decreased SSTs in the Pacific sector, which in turn are consistent with equatorward Ekman transport and negative surface heat fluxes.

While we have hypothesized that the observed-model discrepancies in Antarctic sea ice trends arise from shortcomings in the model and not solely from internal variability, we do not claim to have solved the problem. A true solution would involve improving the CESM and other models of its class, and this requires identifying what aspects of the model are most critical to the response of sea ice to external climate forcing. A good starting place is likely the ocean's thermal structure, as discussed by Armour and Bitz (2015) and Kostov et al. (2016). Compared to observations (Fig. 12a), the annual, zonal-mean mixed layer depths in CESM 1.1 are too shallow, as can be inferred from the shallower isotherms in CESM 1.1 compared to EN4 (Fig. 12b). This shallow mixed layer bias is common among CMIP5 models (e.g. Sallée et al. 2013; Huang et al. 2014). Between ~40°S and ~60°S, the upper ~100 m of the ocean is too warm and buoyant, due in part to the excessive cloud radiative forcing over this region (e.g. Schneider and Reusch 2016). This bias, which may be caused by weak vertical mixing (Huang et al. 2014), limits the model's ability to store excess heat from greenhouse warming deep in the mixed layer. In the polar ocean, underlying the seasonal ice cover, the upper ~100 m is too cold, and the layers between ~100 and ~500 m are too warm (Fig. 12b). The excessive vertical temperature gradient that these biases imply has an important bearing on the model's response to wind forcing. While the above results show that the model does reasonably well with surface processes such as Ekman transport and air–sea heat fluxes, the vertical temperature gradient may determine how quickly the surface response to stronger winds transitions from a cooling driven by surface processes to a warming driven by upwelling of relatively warm waters at depth (Kostov et al. 2016). In CESM, this transition happens

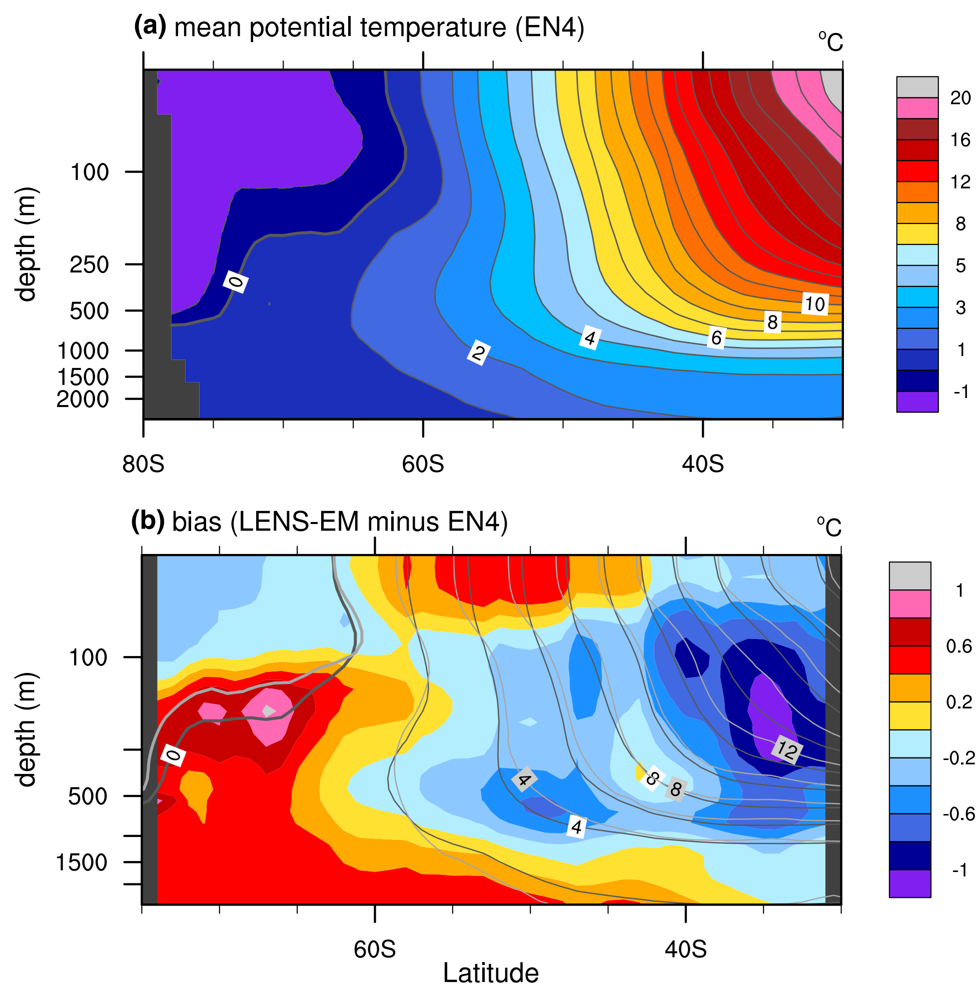

Fig. 12 **a** Climatology of annual-mean, zonal-mean potential temperature in the Southern Ocean according to the EN4 dataset. **b** Model bias in annual-mean, zonal-mean potential temperature in the Southern Ocean, calculated as the difference of the observations and the ensemble mean of the LENS experiment. The *black contours* are the mean isotherms from the observed dataset and the *gray contours* are the mean isotherms from the LENS

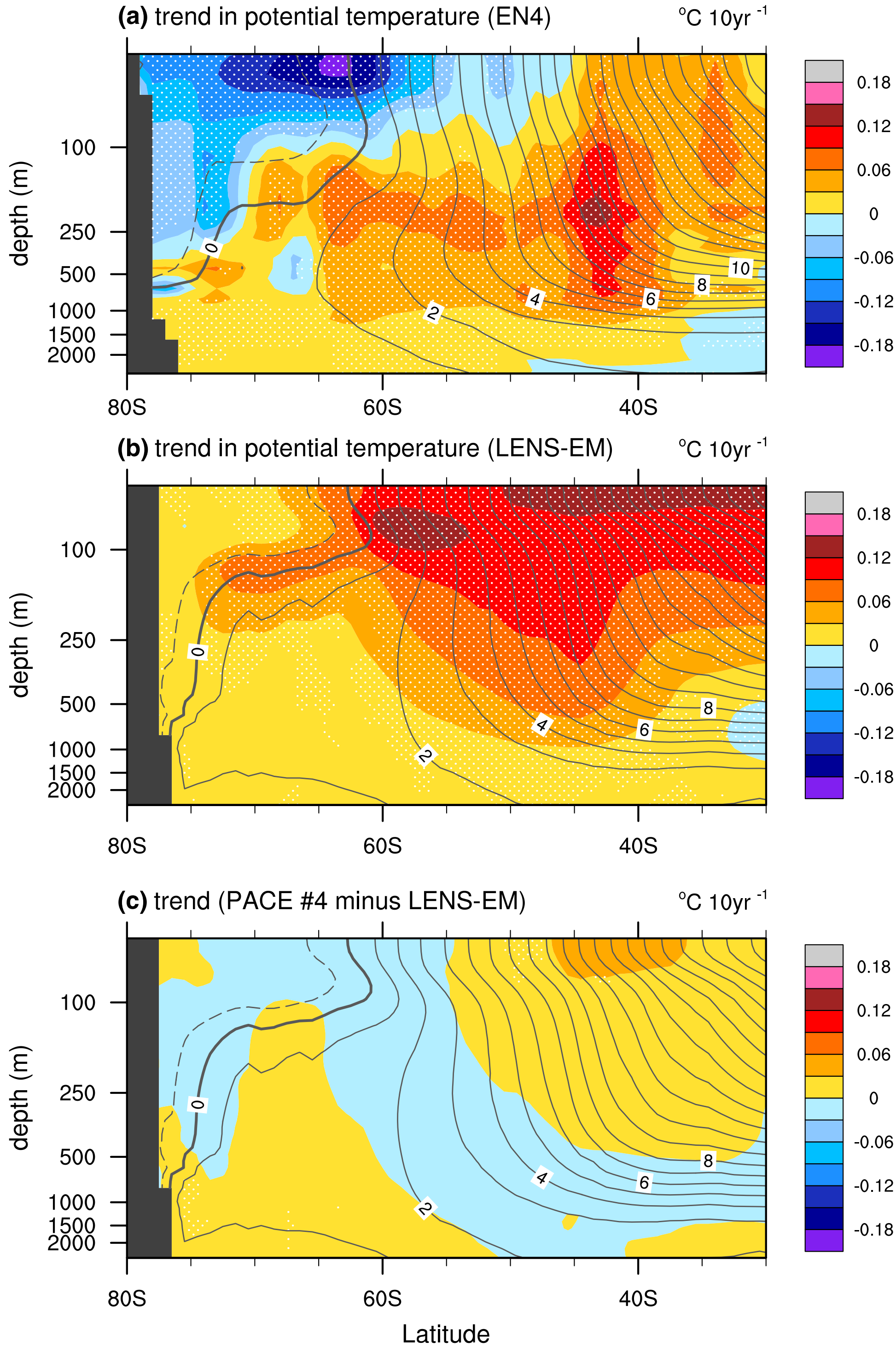

Fig. 13 Trends in annual-mean, zonal-mean potential temperature in the Southern Ocean during 1979–2013 according to **a** the EN4 observational dataset, **b** the ensemble mean of the LENS, and **c** the difference of PACE #4 and the ensemble mean of the LENS. The *black contours* are the mean isotherms from the observations for panel a and the LENS for **b, c**. *Stippling* indicates that the local zonal-mean temperature trend is significant at or above the 90% level

relatively quickly, within a few years of the imposed wind forcing (Ferriera et al. 2015; Kostov et al. 2016).

The trends in ocean potential temperature suggest that the ocean plays a very important role in the forced response as given by the ensemble-mean of the LENS (Fig. 13b). The entire Southern Ocean warms, especially the upper ocean. This warming pattern is very consistent across ensemble members, creating an environment that is not conducive to sea ice expansion. By contrast, the ocean potential temperature trends in the residual are rather weak (Fig. 13c), suggesting that the ocean plays little role in the anomalous sea ice expansion, consistent with the idea that surface processes are the dominant cause. In observations, the Southern Ocean has warmed most at the base of the mixed layer between 40°–60°S, and cooled in the polar surface ocean (Fig. 13a). This observed pattern has been interpreted as the response to stronger westerly winds (Armour and Bitz 2015), with anomalous surface currents transporting cold polar waters northwards to about 45°S, inducing a divergence of surface waters that drives anomalous upwelling south of ~55°S. As ocean temperatures increase with depth in this region (Fig. 12a), these upwelled waters are relatively warm. Counteracting this process, increased sea ice extent and spring melt has contributed to the freshening of the surface ocean (Haumann et al. 2016), which increases buoyancy and reduces the entrainment of warm deepwater into the mixed layer. Thus, the freshening effect of increased sea ice is a mechanism that can delay the "slow response" to stronger winds discussed by Kostov et al. (2016). North of about 45°S, the wind trends have driven anomalous convergence and enhanced subduction, driving anomalous heat into the mixed layer.

The observed ocean potential temperature trend may also bear the signature of the long-term response to greenhouse warming, typically described as the delayed Southern Ocean warming mechanism (e.g. Armour et al. 2016; Marshall et al. 2014; Manabe et al. 1990), in which the Southern Ocean poleward of the Antarctic Circumpolar Current warms more slowly than the rest of the global ocean. This pattern is hinted at in the CESM's forced response (Fig. 13b) in that the ocean warms relatively little polewards of 60°S compared to the warming in the mid-latitudes. Indeed, the warming pattern in Fig. 13b resembles the temperature perturbation that is explicitly attributed to increased atmospheric greenhouse gas concentration in Marshall et al. (2014; see their Fig. 4b). While simulated by models (Marshall et al. 2014; Armour et al. 2016), the delayed warming pattern does not seem adequate to explain the Southern Ocean surface cooling and sea ice expansion of the past several decades. To explain these trends, it is tempting to invoke internal variability, which, according to the model results, could produce an Antarctic sea ice extent trend of the same sign and similar magnitude as the observed trend in the absence of external forcing. Yet the observed increase has occurred in the context of externally forced climate change, and models are not necessarily giving the correct Southern Ocean responses (in rate, spatial pattern, and/or sign) to stronger westerlies (driven by ozone depletion) nor to increased greenhouse gases. The question remains: "What is the true forced response, and what role has it played in the Southern Ocean climate trends of the past several decades relative to internal variability?" To address this question, more work is needed to understand the role of ocean dynamics in the observed and modeled sea ice trends.

In summary, our results suggest that the observed-model discrepancy in Antarctic sea ice trends since 1979 is not simply a matter of internal variability (e.g. Polvani and Smith 2013) that is masking the forced response. Nor is the data-model mismatch solely attributable to the fact that most historical coupled model simulations do not simulate the observed sequence of tropical Pacific variability, including the recent shift in phase of the IPO and PDO (Purich et al. 2016; Meehl et al. 2016). In CESM1, sea ice loss is likely in historical climate change experiments given the strong ocean warming in response to external radiative forcing (e.g. Fig. 13b), combined with a relatively fast increase in polar SSTs (after a ~3-year initial cooling) associated with to stronger westerlies (e.g. Kostov et al. 2016). However, if we allow for internal variability, as well as uncertainty in the responses to greenhouse gasses and stronger westerlies, then we can explain the disagreement of observed and modeled trends. Improving the mean state of the Southern Ocean, particularly with respect to temperature biases and mixing processes, may be the key to achieving more reliable Antarctic sea ice and climate change simulations.

Acknowledgements The authors thank the CESM Climate Variability and Change Working Group (CVCWG, http://www.cesm.ucar.edu/working_groups/CVC/) and Dr. Tingting Fan for conducting and post-processing the CESM1 Tropical Pacific Pacemaker simulations. The CESM Large Ensemble Community Project provided the LENS data. Both experiments benefited from computing resources on Yellowstone managed by NCAR-CISL and sponsored by the National Science Foundation. Drs. David Bailey, Marika Holland and Laura Landrum provided valuable discussions during the course of this work. D. Schneider was supported through NCAR and by National Science Foundation Grant 1235231. The figures were produced with the NCAR Command Language Software Package. NCAR is sponsored by the National Science Foundation. The authors also thank the individual climate modeling groups that have produced and made available the CMIP5 model output, as well as the coordination of those experiments by the World Climate Research Program's Working Group on Coupled Modeling, and the software infrastructure for distributing model data supported by the U.S. Department of Energy's Program for Climate Model Diagnosis and Intercomparison. Finally, the authors thank two anonymous reviewers and the editor for constructive comments that led to an improved manuscript.

References

Agosta C, Fettweis X, Datta R (2015) Evaluation of the CMIP5 models in the aim of regional modelling of the Antarctic surface mass balance. Cryosphere 9:2311–2321. doi:10.5194/tc-9-2311-2015

Armour KC, Bitz CM (2015) Observed and projected trends in Antarctic Sea Ice. US CLIVAR Var 13:12–19

Armour KC, Marshall J, Scott JR et al (2016) Southern Ocean warming delayed by circumpolar upwelling and equatorward transport. Nat Geosci 9:549–554. doi:10.1038/ngeo2731

Bintanja R, van Oldenborgh GJ, Drijfhout SS et al (2013) Important role for ocean warming and increased ice-shelf melt in Antarctic sea-ice expansion. Nat Geosci 6:376–379. doi:10.1038/ngeo1767

Bracegirdle TJ, Stephenson DB, Turner J, Phillips T (2015) The importance of sea ice area biases in 21st century multimodel projections of Antarctic temperature and precipitation. Geophys Res Lett 42:10832–10839. doi:10.1002/2015GL067055

Cionni I, Eyring V, Lamarque JF et al (2011) Ozone database in support of CMIP5 simulations: results and corresponding radiative

forcing. Atmos Chem Phys 11:11267–11292. doi:10.5194/acp-11-11267-2011
Dee D, Uppala S, Simmons A et al (2011) The ERA- Interim reanalysis: configuration and performance of the data assimilation system. Quaterly J R Meteorological Soc 137(656):553–597. doi:10.1002/qj.828
Eisenman I, Meier WN, Norris JR (2014) A spurious jump in the satellite record: has Antarctic sea ice expansion been overestimated? Cryosphere 8:1289–1296. doi:10.5194/tc-8-1289-2014
England MH, McGregor S, Spence P et al (2014) Recent intensification of wind-driven circulation in the Pacific and the ongoing warming hiatus. Nat Clim Change 4:222–227. doi:10.1038/nclimate2106
Fan T, Deser C, Schneider DP (2014) Recent Antarctic sea ice trends in the context of Southern Ocean surface climate variations since 1950. Geophys Res Lett 41:2419–2426. doi:10.1002/2014GL059239
Ferreira D, Marshall J, Bitz CM et al (2015) Antarctic Ocean and sea ice response to ozone depletion: a two-time-scale problem. J Clim 28:1206–1226. doi:10.1175/JCLI-D-14-00313.1
Gettelman A, Kay JE, Fasullo JT et al (2013) Spatial decomposition of climate feedbacks in the community earth system model. J Clim 26:3544–3561. doi:10.1175/JCLI-D-12-00497.1
Good SA, Martin MJ, Rayner NA (2013) EN4: Quality controlled ocean temperature and salinity profiles and monthly objective analyses with uncertainty estimates. J Geophys Res Ocean 118:6704–6716. doi:10.1002/2013JC009067
Haumann FA, Gruber N, Münnich M et al (2016) Sea-ice transport driving Southern Ocean salinity and its recent trends. Nature 537:89–92. doi:10.1038/nature19101
Hobbs WR, Bindoff NL, Raphael MN et al (2015) New perspectives on observed and simulated Antarctic sea ice extent trends using optimal fingerprinting techniques*. J Clim 28:1543–1560. doi:10.1175/JCLI-D-14-00367.1
Hobbs WR, Massom R, Stammerjohn S et al (2016) A review of recent changes in Southern Ocean sea ice, their drivers and forcings. Glob Planet Change 143:228–250. doi:10.1016/j.gloplacha.2016.06.008
Holland PR, Kwok R (2012) Wind-driven trends in Antarctic sea-ice drift. Nat Geosci 5:872–875. doi:10.1038/ngeo1627
Holland MM, Bailey DA, Briegleb BP et al (2012) Improved sea ice shortwave radiation physics in CCSM4: the impact of melt ponds and aerosols on Arctic sea ice*. J Clim 25:1413–1430. doi:10.1175/JCLI-D-11-00078.1
Huang CJ, Qiao F, Dai D (2014) Evaluating CMIP5 simulations of mixed layer depth during summer. J Geophys Res Ocean 119:2568–2582. doi:10.1002/2013JC009535
Hunke EC, Lipscomb WH (2008) CICE: the Los Alamos sea ice model, documentation and software, version 4.0. Los Alamos National Laboratory Technical Report LA-CC-06-012, p 76
Hurrell JW, Holland MM, Gent PR et al (2013) The Community earth system model: a framework for collaborative research. Bull Am Meteorol Soc 94:1339–1360. doi:10.1175/BAMS-D-12-00121.1
Jones JM, Gille ST, Goosse H et al (2016) Assessing recent trends in high-latitude Southern Hemisphere surface climate. Nat Clim Change 6:917–926. doi:10.1038/nclimate3103
Kay JE, Deser C, Phillips A et al (2014) The community earth system model (CESM) large ensemble project: a community resource for studying climate change in the presence of internal climate variability. Bull Am Meteorol Soc. doi:10.1175/BAMS-D-13-00255.1
Kimura N (2004) Sea ice motion in response to surface wind and ocean current in the Southern Ocean. J Meteorol Soc Japan 82:1223–1231. doi:10.2151/jmsj.2004.1223
Kosaka Y, Xie S-P (2013) Recent global-warming hiatus tied to equatorial Pacific surface cooling. Nature 501:403–407. doi: 10.1038/nature12534
Kostov Y, Marshall J, Hausmann U et al (2016) Fast and slow responses of Southern Ocean sea surface temperature to SAM in coupled climate models. Clim Dyn 1–15. doi:10.1007/s00382-016-3162-z
Liu J, Curry JA, Martinson DG (2004) Interpretation of recent Antarctic sea ice variability. Geophys Res Lett. doi:10.1029/2003GL018732
Manabe S, Bryan K, Spelman MJ (1990) Transient response of a global ocean-atmosphere modelto a doubling of atmospheric carbon dioxide. J Phys Oceanogr. doi:10.1175/1520-0485(1990)020<0722:TROAGO>2.0.CO;2
Marsh DR, Mills MJ, Kinnison DE et al (2013) Climate change from 1850 to 2005 simulated in CESM1(WACCM). J Clim 26:7372–7391. doi:10.1175/JCLI-D-12-00558.1
Marshall J, Armour KC, Scott JR et al (2014) The ocean's role in polar climate change: asymmetric Arctic and Antarctic responses to greenhouse gas and ozone forcing. Philos Trans A Math Phys Eng Sci 372:20130040. doi:10.1098/rsta.2013.0040
Matear RJ, O'Kane TJ, Risbey JS et al (2015) Sources of heterogeneous variability and trends in Antarctic sea-ice. Nat Commun 6:8656. doi:10.1038/ncomms9656
Meehl GA, Arblaster JM, Bitz CM et al (2016) Antarctic sea-ice expansion between 2000 and 2014 driven by tropical Pacific decadal climate variability. Nat Geosci 9:590–595. doi:10.1038/ngeo2751
Meier WF, Fetterer F, Savoie M, Mallory S, Duerr R, Stroeve J (2013) NOAA/NSIDC climate data record of passive microwave sea ice concentration, Version 2. NSIDC: National Snow and Ice Data Center, Boulder. doi:10.7265/N55M63M1 **(Updated 2016)**
Parkinson CL, DiGirolamo NE (2016) New visualizations highlight new information on the contrasting Arctic and Antarctic sea-ice trends since the late 1970s. Remote Sens Environ 183:198–204. doi:10.1016/j.rse.2016.05.020
Peng G, Meier WN, Scott DJ, Savoie MH (2013) A long-term and reproducible passive microwave sea ice concentration data record for climate studies and monitoring. Earth Syst Sci Data 5:311–318. doi:10.5194/essd-5-311-2013
Polvani LM, Smith KL (2013) Can natural variability explain observed Antarctic sea ice trends? New modeling evidence from CMIP5. Geophys Res Lett 40:3195–3199. doi:10.1002/grl.50578
Purich A, England MH, Cai W et al (2016) Tropical pacific SST drivers of recent Antarctic sea ice trends. J Clim 29:8931–8948. doi:10.1175/JCLI-D-16-0440.1
Raphael MN, Marshall GJ, Turner J et al (2016) The Amundsen sea low: variability, change, and impact on antarctic climate. Bull Am Meteorol Soc 97:111–121. doi:10.1175/BAMS-D-14-00018.1
Sallée J-B, Shuckburgh E, Bruneau N et al (2013) Assessment of Southern Ocean mixed-layer depths in CMIP5 models: Historical bias and forcing response. J Geophys Res Ocean 118:1845–1862. doi:10.1002/jgrc.20157
Santer BD, Wigley TML, Boyle JS et al (2000) Statistical significance of trends and trend differences in layer-average atmospheric temperature time series. J Geophys Res 105:7337. doi:10.1029/1999JD901105
Schneider DP, Reusch DB (2016) Antarctic and Southern Ocean surface temperatures in CMIP5 models in the context of the surface energy budget*. J Clim 29:1689–1716. doi: 10.1175/JCLI-D-15-0429.1
Schneider DP, Deser C, Fan T et al (2015) Comparing the impacts of tropical SST variability and polar stratospheric ozone loss on the Southern Ocean westerly winds*. J Clim 28:9350–9372. doi:10.1175/JCLI-D-15-0090.1
Sigmond M, Fyfe JC (2014) The antarctic sea ice response to the ozone hole in climate models. J Clim 27(3):1336–1342. doi:10.1175/JCLI-D-13-00590.1
Simpkins GR, Ciasto LM, England MH (2013) Observed variations in multidecadal Antarctic sea ice trends during 1979–2012. Geophys Res Lett 40:3643–3648. doi:10.1002/grl.50715

Smith TM, Reynolds RW, Peterson TC et al (2008) Improvements to NOAA's historical merged land–ocean surface temperature analysis (1880–2006). J Clim 21:2283–2296. doi:10.1175/2007JCLI2100.1

Swart NC, Fyfe JC (2013) The influence of recent Antarctic ice sheet retreat on simulated sea ice area trends. Geophys Res Lett 40:4328–4332. doi:10.1002/grl.50820

Tan I, Storelvmo T, Zelinka MD (2016) Observational constraints on mixed-phase clouds imply higher climate sensitivity. Science 352:224–227. doi:10.1126/science.aad5300

Taylor KE, Stouffer RJ, Meehl GA (2012) An overview of CMIP5 and the experiment design. Bull Am Meteorol Soc 93:485–498. doi:10.1175/BAMS-D-11-00094.1

Trenberth KE, Fasullo JT (2010) Simulation of present-day and twenty-first-century energy budgets of the Southern Oceans. J Clim 23:440–454. doi:10.1175/2009JCLI3152.1

Trenberth KE, Fasullo JT, Branstator G, Phillips AS (2014) Seasonal aspects of the recent pause in surface warming. Nat Clim Change 4:911–916. doi:10.1038/nclimate2341

Turner J, Bracegirdle TJ, Phillips T et al (2013) An initial assessment of Antarctic sea ice extent in the CMIP5 models. J Clim 26:1473–1484. doi:10.1175/JCLI-D-12-00068.1

Turner J, Hosking JS, Marshall GJ et al (2016) Antarctic sea ice increase consistent with intrinsic variability of the Amundsen sea low. Clim Dyn 46:2391–2402. doi:10.1007/s00382-015-2708-9

Xie SP, Deser C, Vecchi GA et al (2010) Global Warming pattern formation: sea surface temperature and rainfall. J Clim 23:966–986. doi:10.1175/2009jcli3329.1

Yeo S-R, Kim K-Y (2015) Decadal changes in the Southern Hemisphere sea surface temperature in association with El Niño–Southern Oscillation and Southern Annular Mode. Clim Dyn 45:3227–3242. doi:10.1007/s00382-015-2535-z

Zunz V, Goosse H, Massonnet F (2013) How does internal variability influence the ability of CMIP5 models to reproduce the recent trend in Southern Ocean sea ice extent? Cryosph 7:451–468. doi:10.5194/tc-7-451-2013